Plasma membrane localization of the mu-opioid receptor controls spatiotemporal signaling

Michelle L. Halls[1], Holly R. Yeatman[1], Cameron J. Nowell[1], Georgina L. Thompson[1], Arisbel Batista Gondin[1], Srgjan Civciristov[1], Nigel W. Bunnett[1,2,3,4], Nevin A. Lambert[6], Daniel P. Poole[1,5] & Meritxell Canals[1,2]

[1]Drug Discovery Biology Theme and [2]ARC Center of Excellence in Convergent Bio-Nano Science and Technology, Monash Institute of Pharmaceutical Sciences and [3]Department of Anesthesia and Perioperative Medicine, Monash University, Australia; [4]Department of Pharmacology and [5]Department of Anatomy and Neuroscience, The University of Melbourne, Australia; [6]Georgia Regents University, Georgia, USA.

Co-corresponding authors: Michelle L Halls (michelle.halls@monash.edu) and Meritxell Canals (meri.canals@monash.edu)

One sentence summary: Ligand-dependent redistribution of MOPr within the plasma membrane controls its spatiotemporal signaling profiles.

Abstract

Differential regulation of the μ-opioid receptor (MOPr) contributes to the clinically limiting effects of opioid analgesics, such as morphine. However, whether differential regulation of MOPr impacts on the spatiotemporal characteristics of receptor activation is unclear. Here we used biophysical approaches to quantify MOPr spatiotemporal signaling. Morphine caused a Gβγ-dependent increase in membrane-localized PKC activity, which restricted the distribution of MOPr within the plasma membrane and induced sustained cytosolic extracellular signal-regulated kinase (ERK). In contrast, DAMGO ([D-Ala^2,N-Me-Phe^4,Gly^5-ol]-enkephalin) allowed receptor redistribution, transient increases in cytosolic and nuclear ERK, and then receptor internalization. Following inhibition of Gβγ-subunits, PKCα or mutation of a key phosphorylation site, the morphine-activated MOPr is released from its restricted localization and stimulates a transient increase in cytosolic and nuclear ERK in the absence of β-arrestin recruitment and internalization. Thus, ligand-induced redistribution of MOPr at the plasma membrane, and not internalization, controls its spatiotemporal signaling.

Introduction

G protein-coupled receptors (GPCRs) are the largest family of cell surface signaling proteins encoded by the human genome. They allow cells to respond to structurally diverse endogenous and environmental signals, and are the target of over 30% of marketed drugs. It is increasingly recognized that the uniform elevation of second messengers throughout the cell cannot explain the diversity of GPCR-mediated effects. Rather, spatial (location) and temporal (duration) control of signaling plays an important role *(1, 2)*. Spatial compartmentalization of signaling can be achieved by the formation of GPCR-dependent protein complexes, which ultimately restrict second messenger diffusion to induce extremely localized signals *(3)*. In addition, multiple regulatory mechanisms (including receptor phosphorylation, desensitization and internalization) control the duration of GPCR activation. Therefore, the spatial and temporal distribution of both receptors and signaling effectors are critical for the generation of distinct and highly specialized GPCR-mediated responses.

The μ-opioid receptor (MOPr) has been extensively studied due to its physiological importance in mediating the effects of endogenous opioids, and its prominence as the target of opioid analgesics, such as morphine. Despite this, chronic use of opioid analgesics is still clinically limited by the development of tolerance, addiction, constipation and respiratory depression *(4)*. At a cellular level, stimulation of MOPr by all opioids activates the same G protein-dependent signaling pathways. MOPr activates $G\alpha_{i/o}$ proteins leading to an inhibition of cAMP, increased ERK phosphorylation, activation of G protein-regulated inwardly rectifying potassium channels, and inhibition of voltage-gated calcium channels *(5)*. However, different MOPr agonists induce distinct patterns of receptor regulation and internalization. In particular, morphine causes limited receptor phosphorylation and β-arrestin recruitment, which results in compromised receptor internalization and resensitization *(6-10)*. These observations have prompted intensive studies of the ability of MOPr ligands to differentially activate G proteins and β-arrestins, in an effort to explain their divergent biological effects *(11-13)*.

It is now apparent that the spatiotemporal characteristics of a signal can specify the outcome of receptor activation *(1, 2)*. Most opioids, including morphine, elicit cytosolic ERK phosphorylation *(14-16)*. However,

unlike other opioids, morphine is unable to promote nuclear ERK phosphorylation *(15)*. Taken together with its impaired internalization of MOPr, this suggests that morphine may stimulate a unique spatiotemporal cellular response. To investigate this, we used complimentary biophysical techniques and super-resolution microscopy. We report that morphine and DAMGO activate distinct spatial and temporal signaling profiles that are controlled by the plasma membrane localization of MOPr induced by the two ligands. Subcellular-targeted Förster Resonance Energy Transfer (FRET) biosensors showed that only morphine stimulation of MOPr induced sustained cytosolic ERK and plasma membrane-localized PKC activation, which restricted MOPr localization. In contrast, DAMGO caused MOPr redistribution within the plasma membrane and transient activation of cytosolic and nuclear ERK. Thus, not only do morphine and DAMGO stimulate different signaling pathways, they activate signals in distinct subcellular compartments with unique temporal profiles. Importantly, we can alter the spatiotemporal signaling profile of morphine to mimic that of DAMGO, by allowing redistribution of MOPr within the plasma membrane in the absence of β-arrestin recruitment or receptor internalization. Thus, receptor localization within the plasma membrane determines the spatiotemporal signals activated by MOPr in response to different ligands.

Results

Ligand-dependent spatiotemporal signaling of MOPr

To gain spatial and temporal resolution of MOPr signaling in live cells, we used FRET biosensors for ERK and PKC (EKAR and CKAR, respectively) localized to different subcellular compartments *(17, 18)*. In HEK293 cells co-transfected with MOPr and either a cytosolic or nuclear ERK biosensor (cytoEKAR, nucEKAR), EC_{50} concentrations of DAMGO (10 nM) or morphine (100 nM; fig. S1A) caused distinct temporal ERK profiles. DAMGO caused a transient increase in cytosolic ERK, whereas morphine induced a sustained increase (Fig. 1, A and B). Moreover, only DAMGO caused a transient increase in nuclear ERK (Fig. 1, C and D). Ligand-dependent responses were also observed when assessing direct activation of PKC. In cells co-transfected with MOPr and a plasma membrane PKC biosensor (pmCKAR) only morphine caused a sustained increase in PKC activity (Fig. 1E). DAMGO did not affect plasma membrane PKC activity, even at maximal concentrations (1 μM; fig. S1B), and neither ligand affected cytosolic PKC (Fig. 1F).

The distinct internalization profiles of MOPr in response to DAMGO and morphine *(6, 10)*, were quantified using a Bioluminescence Resonance Energy Transfer (BRET) assay that detects the proximity between BRET partners in defined subcellular compartments in live cells *(19, 20)*. In agreement with previous reports, incubation with DAMGO (1 μM, fig. S2A) induced MOPr internalization as shown by the increase in the BRET signal between a *Renilla* luciferase-tagged MOPr (MOPr-RLuc) and a Venus-tagged marker of early endosomes (Rab5a-Venus) (Fig. 2A). In contrast, morphine produced no detectable change in BRET (Fig. 2A and fig. S2B). These results were validated by automated, high-content image analysis (fig. S2C). DAMGO-mediated MOPr endocytosis was unaffected by $G\alpha_{i/o}$ inhibition using NF023 or pertussis toxin (PTx) *(21, 22)* but was abolished by the clathrin-dependent endocytosis inhibitor PitStop2 *(23)*, expression of a dominant negative dynamin (K44E) *(24)* or by knockdown of β-arrestins (combined β-arrestin-1 and β-arrestin-2 siRNA; Fig. 2, A and B and fig. S2, D to H). This shows that β-arrestin recruitment and MOPr endocytosis are independent of $G\alpha_{i/o}$ coupling.

Previous studies have linked activation of PKC to cytosolic ERK, and β-arrestin to increased nuclear ERK, to conclude that G protein- and β-arrestin-dependent pathways activate distinct ERK signaling *(15)*. By inhibiting $G\alpha_{i/o}$ proteins, we now directly demonstrate that cytosolic ERK in response to DAMGO and morphine is dependent on $G\alpha_{i/o}$ (Fig. 2C). In agreement with previous studies, cytosolic ERK was unaffected by knockdown of β-arrestins (Fig. 2C). However, inhibition of receptor endocytosis by PitStop2 or dynamin K44E transformed the profile of DAMGO-induced cytosolic ERK from a transient to a sustained signal, consistent with MOPr retention at the plasma membrane (Fig. 2D and fig. S2, I and J). As expected, the increase in nuclear ERK in response to DAMGO was dependent on β-arrestins and receptor internalization (Fig. 2, E and F).

Thus, our results show that $G\alpha_{i/o}$ activation by MOPr mediates increases in cytosolic ERK in response to DAMGO and morphine, and confirm that the increases in nuclear ERK in response to DAMGO are dependent on β-arrestins and receptor endocytosis.

PKC activation controls the ERK spatiotemporal profile of morphine

Inhibition of $G\alpha_{i/o}$ (NF023 or PTx) or Gβγ-subunits (mSIRK or expression of βARKct) *(25, 26)* abolished the plasma membrane PKC response to morphine (Fig. 3A). There was no effect of knockdown of β-arrestins, or negative controls (inactive mSIRK L9A, scrambled siRNA; Fig. 3A and fig. S3A). Thus, the sustained increase in plasma membrane PKC induced by morphine is mediated by $G\alpha_{i/o}$-Gβγ.

Previous studies have reported that PKC activity mediates increased cytosolic ERK in response to morphine *(15)*. We therefore investigated whether the $G\alpha_{i/o}$-Gβγ-PKC pathway influences the unique ERK spatiotemporal signaling profiles of MOPr. Rather than decreasing ERK, and in contrast to previous reports, inhibition of Gβγ-subunits or PKC (GF109203X, Gö6983) *(27, 28)* transformed the temporal profile of morphine-stimulated cytosolic ERK to resemble the transient response induced by DAMGO (Fig. 3B and fig. S3B). Moreover, inhibition of the Gβγ-PKC pathway also allowed morphine to increase nuclear ERK (Fig. 3, C and D). Previous studies have implicated PKCα, PKCγ and PKCε as the isoforms that contribute to morphine signaling and to the

development of morphine tolerance *(16, 29-32)*. Of these, only PKCα and PKCε are expressed in our HEK293 cell line (Fig. S3D). Inhibition of PKCα (Gö6976: targets PKCα and PKCβ$_1$) *(33)* but not PKCε (iPKCε peptide, a cell-permeable PKCε-inhibitory peptide) *(34)* transformed the temporal profile of morphine-stimulated cytosolic ERK and facilitated an increase in nuclear ERK (fig. S3, E and F). There was no effect of inactive controls or of these inhibitors on the response to DAMGO (Fig. 3, B to D and fig. S3, C and F).

As expected, inhibition of Gβγ-subunits or PKC had no effect on β-arrestin-2 recruitment or MOPr internalization induced by DAMGO, determined by BRET or high-content imaging (Fig. 3E and fig. S3, G to I). In contrast, upon inhibition of Gβγ-subunits or PKC, morphine activation of MOPr resulted in a decrease in BRET between MOPr-RLuc and the plasma membrane marker KRas-Venus (Fig. 3F) suggesting an increase in the distance between these two proteins. In the absence of MOPr internalization (Fig. 3E and fig. S3, G to H), the morphine-stimulated change in MOPr-KRas BRET may indicate a movement of the receptor away from KRas *within* the plasma membrane. Thus, the transient activation of cytosolic and nuclear ERK elicited by morphine does not require MOPr internalization but may instead depend on MOPr translocation within the plasma membrane.

The importance of MOPr localization within the plasma membrane for the control of spatiotemporal signaling was also supported by the effects observed upon expression of a phosphorylation-impaired MOPr mutant (S375A) *(35)*. MOPr S375A still recruited β-arrestin-2 in response to DAMGO, but was unable to internalize as determined by high-content imaging or Rab5a BRET (Fig. 3, G and H and fig. S3, G and H). There was no change in MOPr S375A-KRas BRET in response to DAMGO or morphine (fig. S3J). However, stimulation of MOPr S375A by both DAMGO and morphine induced transient increases in cytosolic and nuclear ERK (Fig. 3I and fig. S3K). To confirm that receptor phosphorylation was key for the control of MOPr plasma membrane localization and spatiotemporal signaling, we used a phosphorylation-deficient MOPr mutant in which all the C-terminal Ser and Thr residues have been mutated to Ala (11ST/A) *(9)*. Consistent with previous reports, MOPr 11ST/A was unable to internalize as determined by Rab5a BRET, or recruit β-arrestin-2 in response to DAMGO

(Fig. 3, G and H). However, stimulation of MOPr 11ST/A by both DAMGO and morphine induced a transient increase in nuclear ERK, with no change in KRas BRET (Fig. 3I and fig. S3J). Phosphorylation of Ser375 therefore appears critical for the control of MOPr spatiotemporal signaling in response to morphine. Taken together, these data show that the impaired trafficking of MOPr mutants results in an altered signaling profile and support the hypothesis that the plasma membrane localization of MOPr, and not β-arrestin recruitment or receptor internalization, plays a key role in the spatiotemporal control of receptor signaling.

Ligand-dependent redistribution of MOPr within the plasma membrane

To investigate the changes in MOPr distribution elicited by morphine upon inhibition of the Gβγ-PKCα pathway, we assessed receptor localization at the plasma membrane by confocal microscopy and subcellular fractionation. After 10 min stimulation of MOPr (which causes activation of all signaling pathways) there was no colocalization between the receptor and immunolabeled clathrin by confocal microscopy under any condition tested (fig. S4, A and B). However, after 60 min, stimulation with DAMGO but not morphine caused significant colocalization between MOPr and clathrin (fig. S4C). In contrast, activation of the fast internalizing β_2-adrenoceptor (β_2AR) by isoprenaline caused significant receptor-clathrin colocalization after 10 min (fig. S4, A to C). Similarly, there was no effect of DAMGO or morphine stimulation on the location of FLAG-MOPr within non-lipid-rich (Triton X-100 soluble) plasma membrane domains using basic lipid fractionation (fig. S4D). Therefore, the distinct spatiotemporal signaling profiles of morphine and DAMGO do not reflect ligand-dependent MOPr clustering in clathrin-coated pits nor translocation to different lipid domains.

To investigate MOPr localization within the plasma membrane with increased resolution, we used ground state depletion (GSD) super-resolution microscopy in total internal reflection fluorescence (TIRF) mode. GSD/TIRF allows the detection of events within the plane of the plasma membrane to an axial resolution of 100 nm. This approach can measure the distance between an event (receptor or receptor clusters) and its nearest neighbor across a population. Stimulation of FLAG-MOPr with DAMGO (10 min) increased the average distance between detected events (Fig. 4, A and B), suggesting MOPr redistribution within the plasma membrane. This

increase in distance occurs prior to and is independent of receptor internalization, as there was no effect of expression of dominant negative dynamin K44E (fig. S4, E and F).

Morphine stimulation of FLAG-MOPr (10 min) did not change the average distance between events (Fig. 4, A and B). However, following inhibition of Gβγ-subunits morphine increased the distance between detected MOPr events (Fig. 4, C and D and fig. S4, E and G), suggesting that activation of this pathway by morphine normally restricts MOPr localization. Interestingly, the distance between MOPr events under basal conditions following expression of MOPr S375A was also increased when compared to the wild-type receptor (Fig. 4, E and F). This increase in distance between events was not due to decreased receptor expression at the plasma membrane (MOPr S375A 570,000 sites per cell, MOPr wild-type 140,000 sites per cell measured by whole cell [^{3}H]-diprenorphine binding), confirming that MOPr S375A was differentially distributed compared to the wild-type receptor.

Thus, our results suggest that activation of MOPr by morphine restricts receptor localization, whereas DAMGO stimulation allows MOPr redistribution within the plasma membrane. Disruption of the Gβγ-PKCα-phosphorylation pathway allows morphine to stimulate a DAMGO-like redistribution of MOPr but does not result in receptor internalization. This receptor redistribution precedes (DAMGO), or can occur independently of (morphine), endocytosis and appears to control the ability of MOPr to transiently activate cytosolic and nuclear ERK.

Disruption of plasma membrane organization alters MOPr spatiotemporal signaling

To confirm the importance of membrane organization in the control of compartmentalized MOPr signaling, we depleted cholesterol from the plasma membrane using methyl-β-cyclodextrin (MβCD) *(36)* or Filipin III *(37)*. There was no effect of these treatments on MOPr internalization, as determined by high-content imaging (fig. S5, A and B). However, both MβCD and Filipin III abolished the distinct spatiotemporal signaling profiles of morphine and DAMGO (Fig. 5 and fig. S5). Upon cholesterol depletion, both morphine and DAMGO increased

PKC activity at the plasma membrane and caused a transient increase in cytosolic and nuclear ERK (Fig. 5 and fig. S5, C to F). Importantly, membrane cholesterol replenishment by incubation of the cells with MβCD/cholesterol complexes, completely restored the original spatiotemporal signaling profiles of DAMGO and morphine (Fig. 5 and fig. S5).

Thus, disruption of membrane organization alters the spatiotemporal signaling profiles of MOPr, with no change in the ability of the receptor to internalize, confirming that plasma membrane localization of MOPr plays an important role in determining its spatiotemporal signaling.

MOPr compartmentalized signaling in dorsal root ganglia (DRG) neurons

To confirm the physiological relevance of the spatiotemporal signaling patterns of MOPr when expressed in HEK293 cells, we nucleofected isolated neurons from mouse DRG with the FRET biosensors. DRG neurons are the principal mediators of nociception from the periphery to the spinal cord and activation of endogenous MOPr in these neurons partially mediates the analgesic actions of opioids *(38)*.

Activation of MOPr in DRG neurons stimulated ERK and PKC activity with spatiotemporal profiles that were identical to those observed in HEK293 cells. DAMGO caused a transient increase in both cytosolic and nuclear ERK, whereas morphine elicited a sustained increase in cytosolic ERK and plasma membrane PKC (Fig. 6, A to C). Inhibition of PKC decreased the percentage of neurons that exhibited a sustained cytosolic ERK response to morphine (from 75% to 49%), and increased the percentage of neurons that exhibited a transient cytosolic ERK response (from 25% to 51%) (Fig. 6, D and E). There was no effect of PKC inhibition on the temporal profile of cytosolic ERK following stimulation with DAMGO (Fig. 6, D and E). As observed in HEK293 cells, inhibition of PKC allowed morphine to activate nuclear ERK (Fig. 6F).

We also assessed the distribution of endogenous MOPr at the plasma membrane of DRG neurons (Fig. 6G) using GSD/TIRF microscopy. As in HEK293 cells, stimulation of endogenous MOPr in DRG neurons with DAMGO

increased the distance between detected events at the plasma membrane (Fig. 6, H and I). In contrast, there was no change in the distance between MOPr events in response to morphine.

Thus, in DRG neurons, as in HEK293 cells, receptor redistribution at the plasma membrane correlates with transient increases in cytosolic and nuclear ERK in response to DAMGO. Moreover, inhibition of PKC allows morphine to cause transient increases in cytosolic and nuclear ERK. As such, the spatiotemporal regulation of MOPr activation and signaling identified in recombinant expression systems also occurs in DRG neurons endogenously expressing this receptor.

Discussion

The use of biophysical approaches to assess MOPr signaling in real time and in live cells has revealed a new mechanism that contributes to the control of differential MOPr activation. Here we show that DAMGO activation of MOPr triggers receptor translocation within the plasma membrane. This translocation precedes receptor trafficking to clathrin-containing domains and internalization and is likely dependent on receptor phosphorylation (Fig. 7A). This MOPr translocation, not receptor internalization, determines the transient cytosolic ERK profile and the activation of nuclear ERK (Fig. 7A). In contrast, morphine activates plasma membrane-localized PKCα, via Gβγ-subunits, which prevents receptor translocation within the plasma membrane. This results in sustained cytosolic ERK and no nuclear ERK activity (Fig. 7B). Inhibition of this Gβγ-PKCα-phosphorylation pathway allows the morphine-activated MOPr to translocate within the plasma membrane and transforms its spatiotemporal signaling profile (Fig. 7B). Importantly, this new signaling profile mimics that of the internalizing ligand DAMGO (i.e. transient cytosolic and nuclear ERK) but occurs in the absence of β-arrestin-2 recruitment and without receptor internalization.

These results add essential detail to previous descriptions of ligand-dependent differences in ERK signaling *(14-16)*. Previous studies using immunoblotting showed that etorphine-induced ERK phosphorylation was dependent on β-arrestins, whereas morphine activated ERK via a PKC-dependent pathway *(15)*. However, we show that upon PKC inhibition, morphine can still induce ERK phosphorylation, although this signal has different temporal dynamics and occurs both in the cytosol and the nucleus (Fig. 3 and 7B). Therefore, the activation of cytosolic ERK by morphine is not PKC-dependent but rather PKC, by controlling MOPr localization, dictates the dynamics and location of this response. It is interesting to consider that in the context of a whole cell following solubilization (with a relatively greater contribution of cytosolic compared to nuclear ERK), this altered temporal profile could appear as an apparent *decrease* in morphine stimulated ERK. This illustrates the extra mechanistic detail that can be obtained by resolving spatial and temporal signaling dynamics in live cells. We therefore propose that plasma membrane organization of MOPr, not just β-arrestin recruitment and

internalization, dictates the spatiotemporal outcome of receptor activation. Importantly, these mechanisms operate in nociceptive neurons, and may thus contribute to the analgesic actions of opioids.

The ability of DAMGO, but not morphine, to cause receptor redistribution may relate to differential patterns of MOPr phosphorylation. While all opioids cause phosphorylation of MOPr at Ser375, this is mediated by different kinases depending on the ligand *(9, 39)*. Previous studies have shown that the DAMGO-activated MOPr is phosphorylated by GRKs 2 and 3 and that internalizing ligands drive higher-order phosphorylation of flanking residues that result in efficient β-arrestin recruitment and receptor internalization *(9)*. Here we show that recruitment of β-arrestin-2, MOPr translocation and activation of nuclear ERK in response to DAMGO precede receptor internalization. As such, we hypothesize that differential recruitment of regulatory proteins (GRKs, β-arrestins) to MOPr may underlie receptor redistribution at the plasma membrane, and thus indirectly control spatiotemporal signaling. This is supported by the fact that mutation of the key hierarchical phosphorylation site of MOPr (MOPr S375A) affects the localization of the receptor within the plasma membrane and its spatiotemporal signaling. In this context, β-arrestins are increasingly recognized as scaffolding proteins for signaling complexes, in addition to their traditional roles in the regulation of receptor desensitization and internalization *(40)*. Furthermore, recent evidence suggests that GRKs can also have important scaffolding functions, particularly for the control of ERK activation *(41, 42)*. We hypothesize that differential assembly of receptor kinases and other signaling mediators in response to morphine versus DAMGO stimulation of MOPr determines receptor redistribution, transient signaling profiles and activation of nuclear ERK. Importantly, this entails that the responses of opioid ligands will be highly dependent on the specific protein content of opioid-responsive cells *(6, 7, 43, 44)*.

Our results also highlight the importance of PKCα in governing MOPr spatiotemporal signaling profiles. Previous studies have shown that phosphorylation and desensitization of MOPr following morphine stimulation is partially dependent upon PKC *(39, 45, 46)*. Moreover, there are strong indications that PKC plays a significant role in the initiation and maintenance of tolerance to morphine analgesia *(47, 48)*. To date, evidence for

morphine-induced activation of PKC comes from co-immunoprecipitation studies showing recruitment of over-expressed PKCε to MOPr *(16)* and increased PKC activity in cell lysates *(49)*. By measuring endogenous PKC activity at the subcellular level, we directly demonstrate that morphine, but not DAMGO, stimulates a sustained activation of PKC at the plasma membrane. While PKC can phosphorylate MOPr directly *(32, 50)*, it can also phosphorylate proteins that participate in MOPr signaling such as $G\alpha_i$ *(51)* or GRK2 *(52)* and could therefore restrict receptor redistribution by modulating the function and/or association of such signaling and scaffolding proteins with MOPr.

It is clear that plasma membrane organization plays a critical role in the control of MOPr spatiotemporal signaling. Whether MOPr resides within biochemically-defined lipid-rich plasma membrane regions is controversial *(53-55)*. However, and in line with our findings, previous studies have provided evidence for a restricted plasma membrane localization, and agonist-regulated plasma membrane diffusion of the MOPr *(56-59)*. Protein-protein interactions were hypothesized to mediate the restricted and slow diffusion of agonist-stimulated non-internalizing MOPr *(60)*. Together with the results presented here, this suggests that the dynamic organization of MOPr within the plasma membrane, rather than MOPr association with a pre-defined lipid-rich domain, may control ligand-dependent receptor redistribution and unique spatiotemporal signaling profiles. The dependence of MOPr signaling on plasma membrane localization extends recent studies demonstrating distinct control of spatiotemporal signaling by endosomally-localized GPCRs *(2, 61)*. In the context of MOPr, mechanistic insight into the actions of morphine at the cellular level is of particular therapeutic relevance due to the severe side-effects induced by this opiate. Whether chronic exposure to opiates differentially alters spatiotemporal signaling and/or the plasma membrane distribution of MOPr remains to be investigated.

Materials and Methods

Reagents, cDNAs and methods for Supplementary Figures are described in Supplementary Materials and Methods.

Cell culture and inhibitors

HEK293 cells were grown in DMEM supplemented with 5% v/v FBS. Cells were transfected using linear polyethyleneimine (PEI) *(62)*. For siRNA, cells were transfected with 25 nM scrambled or combined β-arrestin-1 and β-arrestin-2 SMARTpool ON-TARGETplus siRNA with Lipofectamine 2000 24 h prior to transfection with receptor and biosensors.

Cells were pre-treated with inhibitors for 30 min at 37°C, except for Filipin III, MβCD or MβCD/cholesterol complexes (45 min) or PTx (16 hours). MβCD/cholesterol complexes were formed as described previously *(63)*. Inhibitors were used at the following concentrations: 30 μM PitStop2 or inactive PitStop2, 10 μM NF023, 100 ng/mL PTx, 5 μM mSIRK or mSIRK L9A, 1 μM GF109203X or Gö6983, 10 nM Gö6976, 10 μM Myr-EAVSLKPT-OH (inhibitory PKCε peptide, iPKCε), 1 μg/mL Filipin III, 10 mM MβCD, 2 mM MβCD with 0.2 mM cholesterol (MβCD/cholesterol complexes).

All experiments were performed in live cells at 37°C. For all regulation and trafficking experiments cells were stimulated with an EC_{50} concentration of DAMGO or morphine (both 1 μM) defined by β-arrestin-2 concentration-response curves (fig. S2A). For all signaling experiments cells were stimulated with an EC_{50} concentration of DAMGO (10 nM) or morphine (100 nM) defined by AlphaScreen pERK assays (fig. S1A).

DRG isolation and culture

All procedures involving mice were approved by the Monash Institute of Pharmaceutical Sciences animal ethics committee. DRG neurons were isolated and nucleofected with 600 ng of cytoEKAR Cerulean/Venus, nucEKAR

Cerulean/Venus or pmCKAR using the Nucleofector system (Lonza) (see *(62)* for detailed protocols of DRG isolation and nucleofection).

Bioluminescence Resonance Energy Transfer

HEK293 cells were transfected with 1 μg MOPr-RLuc and 4 μg KRas-Venus, Rab5a-Venus or β-arrestin-2-YFP. For co-expression, cells were transfected with an additional 2 μg of βARKct, GFP-dynamin or GFP-dynamin K44E. After 24 hours cells were plated in poly-D-lysine-coated 96-well plates (CulturPlate, PerkinElmer) and allowed to adhere. 48 hours post-transfection, cells were equilibrated in HBSS then stimulated with vehicle (0.1% DMSO), DAMGO or morphine for 30 min. Coelenterazine h (Promega) was added at a final concentration of 5 μM and cells were incubated for 10 min. BRET measurements were obtained using a PHERAstar Omega (BMG Labtech, Germany) that allows sequential integration of the signals detected at 475±30 and 535±30 nm using filters with the appropriate band pass. Data are presented as a BRET ratio (calculated as the ratio of YFP to RLuc signals) corrected for vehicle.

FRET

HEK293 cells were transfected with 55 ng/well MOPr and 40 ng/well cytoEKAR GFP/RFP, nucEKAR GFP/RFP, cytoCKAR or pmCKAR. For co-expression, cells were transfected with an additional 50 ng/well βARKct, GFP-dynamin or GFP-dynamin K44E. Experiments co-expressing GFP-dynamin or GFP-dynamin K44E used the Cerulean/Venus FRET sensors. FRET was measured using a high-content GE Healthcare INCell 2000 Analyzer (see *(62)* for detailed protocols). Briefly, fluorescence imaging was performed using a Nikon Plan Fluor ELWD 40x (NA 0.6) objective and FRET module. For GFP/RFP emission ratio analysis, cells were sequentially excited using a FITC filter (490/20) with emission measured using dsRed (605/52) and FITC (525/36) filters, and a polychroic optimized for the FITC/dsRed filter pair (Quad4). For CFP/YFP or Cerulean/Venus emission ratio analysis, cells were sequentially excited using a CFP filter (430/24) with emission measured using YFP (535/30) and CFP (470/24) filters, and a polychroic optimized for the CFP/YFP filter pair (Quad3). HEK293 cells were imaged every 1 min, allowing image capture of 14 wells per min; DRG

neurons were imaged every 1 min with four fields of view per well, allowing capture of 3 wells per min. At the end of every experiment, the same cells were stimulated with the positive control (200 nM phorbol 12,13-dibutyrate for ERK or 200 nM phorbol 12,13-dibutyrate with phosphatase inhibitor cocktail 2 (Sigma Aldrich) for PKC) for 10 min to generate a maximal FRET change, and positive emission ratio images were captured for 4 min.

Data were analyzed using the FIJI distribution of ImageJ *(64)*. The three emission ratio image stacks (baseline, stimulated, positive) were collated and aligned using the StackCreator script *(62)*. Cells were selected and fluorescence intensity measured over the combined stack. Background intensity was subtracted, then FRET data plotted as the change in FRET emission ratio relative to the maximal response for each cell (FRET ratio/maximum FRET ratio; F/F_{Max}). For HEK293, only cells that showed more than a 10% change relative to baseline following stimulation with the positive control were considered for analysis. For DRG neurons, all cells that showed more than a 3% change relative to baseline following stimulation with the positive control were considered for analysis.

Ratiometric pseudocolor images were generated according to *(65)*. The Green Fire Blue LUT was applied, and the Brightness and Contrast range was set to the minimum and maximum FRET ratios within the image stack (0.13-0.23).

GSD/TIRF microscopy

HEK293 cells and DRG neurons were stimulated with vehicle (0.1% DMSO), DAMGO or morphine as indicated, fixed in 4% paraformaldehyde (20 min, 4°C), washed for 15 min with PBS, blocked in PBS with 1% Normal goat serum and 0.1% saponin (1 hour, RT), and incubated overnight at 4°C with mouse anti-FLAG antibody (1:1000) for HEK293 or rabbit anti-MOPr (UMB-3, 1:250) and anti-tubulin βIII (1:1000) for DRG neurons. Cells were washed and incubated with Alexa568- or Alexa647-conjugated goat anti-mouse or anti-rabbit secondary antibodies (1:400, 2 hours, RT). Coverslips were mounted on a concave slide containing 100

mM cysteamine (MEA) and sealed. Cells were observed with a Leica GSD microscope with HCX PL APO 160x (NA 1.43) objective, SuMo stage, Andor iXon Ultra 897 camera and LAS AF software. Pumping occurred at 100% laser power until the frame correlation dropped to 0.25. Data were acquired at 50% laser power, and up to 30,000 frames captured. TIRF penetration was at 110 nm. Only neurons with positive staining for β-tubulin were analyzed. Images were analyzed in FIJI *(64)*. Individual particles were selected using Find Maxima (noise tolerance 5) to generate a binary output of the single points. The average distance between events was calculated by creating a centroid list using the Analyze Particles command, and processed by the Nearest Neighbor Distance (NND) macro (Yuxiong Mao). Euclidean distance maps were generated from the single point binary image using the Euclidean Distance option.

Supplementary Materials

Supplementary Materials and Methods

Supplementary Figure 1

Supplementary Figure 2

Supplementary Figure 3

Supplementary Figure 4

Supplementary Figure 5

References

1. N. G. Tsvetanova, M. von Zastrow, Spatial encoding of cyclic AMP signaling specificity by GPCR endocytosis, *Nat Chem Biol* **10**, 1061–1065 (2014).

2. D. Calebiro, V. Nikolaev, M. Gagliani, T. de Filippis, C. Dees, C. Tacchetti, L. Persani, M. Lohse, Persistent cAMP-signals triggered by internalized G-protein-coupled receptors, *PLoS Biol* **7**, e1000172 (2009).

3. V. Nikolaev, M. Bunemann, E. Schmitteckert, M. Lohse, S. Engelhardt, Cyclic AMP imaging in adult cardiac myocytes reveals far-reaching β1-adrenergic but locally confined β2-adrenergic receptor-mediated signaling, *Circ Res* **99**, 1084–1091 (2006).

4. K. Ahlbeck, Opioids: a two-faced Janus, *Curr Med Res Opin* **27**, 439–448 (2011).

5. R. Al-Hasani, M. R. Bruchas, Molecular mechanisms of opioid receptor-dependent signaling and behavior, *Anesthesiology* **115**, 1363–1381 (2011).

6. J. L. Whistler, M. von Zastrow, Morphine-activated opioid receptors elude desensitization by β-arrestin, *Proc Natl Acad Sci U S A* **95**, 9914–9919 (1998).

7. J. Zhang, S. S. Ferguson, L. S. Barak, S. R. Bodduluri, S. A. Laporte, P. Y. Law, M. G. Caron, Role for G protein-coupled receptor kinase in agonist-specific regulation of μ-opioid receptor responsiveness, *Proc Natl Acad Sci U S A* **95**, 7157–7162 (1998).

8. N. Quillinan, E. K. Lau, M. Virk, M. von Zastrow, J. T. Williams, Recovery from μ-opioid receptor desensitization after chronic treatment with morphine and methadone, *J Neurosci* **31**, 4434–4443 (2011).

9. S. Just, S. Illing, M. Trester-Zedlitz, E. K. Lau, S. J. Kotowski, E. Miess, A. Mann, C. Doll, J. C. Trinidad, A. L. Burlingame, M. von Zastrow, S. Schulz, Differentiation of opioid drug effects by hierarchical multi-site phosphorylation, *Mol Pharmacol* **83**, 633–639 (2013).

10. D. E. Keith, S. R. Murray, P. A. Zaki, P. C. Chu, D. V. Lissin, L. Kang, C. J. Evans, M. von Zastrow, Morphine activates opioid receptors without causing their rapid internalization, *J Biol Chem* **271**, 19021–19024 (1996).

11. L. M. Bohn, R. J. Lefkowitz, R. R. Gainetdinov, K. Peppel, M. G. Caron, F. T. Lin, Enhanced morphine analgesia in mice lacking β-arrestin 2, *Science* **286**, 2495–2498 (1999).

12. C. E. Groer, K. Tidgewell, R. A. Moyer, W. W. Harding, R. B. Rothman, T. E. Prisinzano, L. M. Bohn, An opioid agonist that does not induce μ-opioid receptor-β-arrestin interactions or receptor internalization, *Mol Pharmacol* **71**, 549–557 (2006).

13. S. M. DeWire, D. S. Yamashita, D. H. Rominger, G. Liu, C. L. Cowan, T. M. Graczyk, X. T. Chen, P. M. Pitis, D. Gotchev, C. Yuan, M. Koblish, M. W. Lark, J. D. Violin, A G protein-biased ligand at the μ-opioid receptor is potently analgesic with reduced gastrointestinal and respiratory dysfunction compared with morphine, *J Pharmacol Exp Ther* **344**, 708–717 (2013).

14. H. Zheng, J. Chu, Y. Qiu, H. H. Loh, P.-Y. Law, Agonist-selective signaling is determined by the receptor location within the membrane domains, *Proc Natl Acad Sci U S A* **105**, 9421–9426 (2008).

15. H. Zheng, H. H. Loh, P.-Y. Law, β-arrestin-dependent μ-opioid receptor-activated extracellular signal-regulated kinases (ERKs) translocate to nucleus in contrast to G protein-dependent ERK activation, *Mol Pharmacol* **73**, 178–190 (2008).

16. H. Zheng, J. Chu, Y. Zhang, H. H. Loh, P. Y. Law, Modulating μ-opioid receptor phosphorylation switches agonist-dependent signaling as reflected in PKC activation and dendritic spine stability, *J Biol Chem* **286**, 12724–12733 (2011).

17. C. D. Harvey, A. G. Ehrhardt, C. Cellurale, H. Zhong, R. Yasuda, R. J. Davis, K. Svoboda, A genetically encoded fluorescent sensor of ERK activity, *Proc Natl Acad Sci U S A* **105**, 19264–19269 (2008).

18. J. D. Violin, J. Zhang, R. Y. Tsien, A. C. Newton, A genetically encoded fluorescent reporter reveals oscillatory phosphorylation by protein kinase C, *J Cell Biol* **161**, 899–909 (2003).

19. T.-H. Lan, Q. Liu, C. Li, G. Wu, N. A. Lambert, Sensitive and high resolution localization and tracking of membrane proteins in live cells with BRET, *Traffic (Copenhagen, Denmark)* **13**, 1450–1456 (2012).

20. D. D. Jensen, C. B. Godfrey, C. Niklas, M. Canals, M. Kocan, D. P. Poole, J. E. Murphy, F. Alemi, G. S. Cottrell, C. Korbmacher, N. A. Lambert, N. W. Bunnett, C. U. Corvera, The bile acid receptor TGR5 does not interact with β-arrestins or traffic to endosomes but transmits sustained signals from plasma membrane rafts, *J Biol Chem* **288**, 22942–22960 (2013).

21. M. Freissmuth, S. Boehm, W. Beindl, P. Nickel, A. P. IJzerman, M. Hohenegger, C. Nanoff, Suramin analogues as subtype-selective G protein inhibitors, *Mol Pharmacol* **49**, 602–611 (1996).

22. T. Katada, M. Ui, Direct modification of the membrane adenylate cyclase system by islet-activating protein due to ADP-ribosylation of a membrane protein, *Proc Natl Acad Sci U S A* **79**, 3129–3133 (1982).

23. L. von Kleist, W. Stahlschmidt, H. Bulut, K. Gromova, D. Puchkov, M. J. Robertson, K. A. MacGregor, N. Tomilin, A. Pechstein, N. Chau, M. Chircop, J. Sakoff, J. P. von Kries, W. Saenger, H.-G. Kräusslich, O. Shupliakov, P. J. Robinson, A. McCluskey, V. Haucke, Role of the clathrin terminal domain in regulating coated pit dynamics revealed by small molecule inhibition, *Cell* **146**, 471–484 (2011).

24. J. S. Herskovits, C. C. Burgess, R. A. Obar, R. B. Vallee, Effects of mutant rat dynamin on endocytosis, *J Cell Biol* **122**, 565–578 (1993).

25. J. K. Scott, S. F. Huang, B. P. Gangadhar, G. M. Samoriski, P. Clapp, R. A. Gross, R. Taussig, A. V. Smrcka, Evidence that a protein-protein interaction "hot spot" on heterotrimeric G protein βγ subunits is used for recognition of a subclass of effectors, *EMBO J* **20**, 767–776 (2001).

26. W. J. Koch, B. E. Hawes, J. Inglese, L. M. Luttrell, R. J. Lefkowitz, Cellular expression of the carboxyl terminus of a G protein-coupled receptor kinase attenuates G βγ-mediated signaling, *J Biol Chem* **269**, 6193–6197 (1994).

27. D. Toullec, P. Pianetti, H. Coste, P. Bellevergue, T. Grand-Perret, M. Ajakane, V. Baudet, P. Boissin, E. Boursier, F. Loriolle, The bisindolylmaleimide GF 109203X is a potent and selective inhibitor of protein kinase C, *J Biol Chem* **266**, 15771–15781 (1991).

28. M. Gschwendt, S. Dieterich, J. Rennecke, W. Kittstein, H. J. Mueller, F. J. Johannes, Inhibition of protein kinase C μ by various inhibitors. Differentiation from protein kinase c isoenzymes, *FEBS Lett* **392**, 77–80 (1996).

29. C. P. Bailey, S. Oldfield, J. Llorente, C. J. Caunt, A. G. Teschemacher, L. Roberts, C. A. McArdle, F. L. Smith, W. L. Dewey, E. Kelly, G. Henderson, Involvement of PKCα and G-protein-coupled receptor kinase 2 in agonist-selective desensitization of μ-opioid receptors in mature brain neurons, *Br J Pharmacol* **158**, 157–164 (2009).

30. M. Inoue, H. Ueda, Protein kinase C-mediated acute tolerance to peripheral μ-opioid analgesia in the bradykinin-nociception test in mice, *J Pharmacol Exp Ther* **293**, 662–669 (2000).

31. F. L. Smith, B. H. Gabra, P. A. Smith, M. C. Redwood, W. L. Dewey, Determination of the role of conventional, novel and atypical PKC isoforms in the expression of morphine tolerance in mice, *Pain* **127**, 129–139 (2007).

32. S. Illing, A. Mann, S. Schulz, Heterologous regulation of agonist-independent μ-opioid receptor phosphorylation by protein kinase C, *Br J Pharmacol* **171**, 1330–1340 (2014).

33. G. Martiny-Baron, M. G. Kazanietz, H. Mischak, P. M. Blumberg, G. Kochs, H. Hug, D. Marmé, C. Schächtele, Selective inhibition of protein kinase C isozymes by the indolocarbazole Gö 6976, *J Biol Chem* **268**, 9194–9197 (1993).

34. J. A. Johnson, M. O. Gray, C. H. Chen, D. Mochly-Rosen, A protein kinase C translocation inhibitor as an isozyme-selective antagonist of cardiac function, *J Biol Chem* **271**, 24962–24966 (1996).

35. S. Schulz, D. Mayer, M. Pfeiffer, R. Stumm, T. Koch, V. Höllt, Morphine induces terminal μ-opioid receptor desensitization by sustained phosphorylation of serine-375, *EMBO J* **23**, 3282–3289 (2004).

36. Y. Ohtani, T. Irie, K. Uekama, K. Fukunaga, J. Pitha, Differential effects of α-, β- and γ-cyclodextrins on human erythrocytes, *Eur J Biochem / FEBS* **186**, 17–22 (1989).

37. A. W. Norman, R. A. Demel, B. de Kruyff, L. L. van Deenen, Studies on the biological properties of polyene antibiotics. Evidence for the direct interaction of filipin with cholesterol, *J Biol Chem* **247**, 1918–1929 (1972).

38. A. I. Basbaum, D. M. Bautista, G. Scherrer, D. Julius, Cellular and molecular mechanisms of pain, *Cell* **139**, 267–284 (2009).

39. C. Doll, J. Konietzko, F. Pöll, T. Koch, V. Höllt, S. Schulz, Agonist-selective patterns of μ-opioid receptor phosphorylation revealed by phosphosite-specific antibodies, *Br J Pharmacol* **164**, 298–307 (2011).

40. K. A. DeFea, β-arrestins as regulators of signal termination and transduction: how do they determine what to scaffold? *Cell Signal* **23**, 621–629 (2011).

41. J. D. Robinson, J. A. Pitcher, G protein-coupled receptor kinase 2 (GRK2) is a Rho-activated scaffold protein for the ERK MAP kinase cascade, *Cell Signal* **25**, 2831–2839 (2013).

42. P. Penela, C. Ribas, I. Aymerich, N. Eijkelkamp, O. Barreiro, C. Heijnen, A. Kavelaars, F. Sanchez-Madrid, F. Mayor, G protein-coupled receptor kinase 2 positively regulates epithelial cell migration, *EMBO J* **27**, 1206–1218 (2008).

43. H. Haberstock-Debic, M. Wein, M. Barrot, E. E. O. Colago, Z. Rahman, R. L. Neve, V. M. Pickel, E. J. Nestler, M. von Zastrow, A. L. Svingos, Morphine acutely regulates opioid receptor trafficking selectively in dendrites of nucleus accumbens neurons, *J Neurosci* **23**, 4324–4332 (2003).

44. H. Haberstock-Debic, Morphine promotes rapid, arrestin-dependent endocytosis of μ-opioid receptors in striatal neurons, *J Neurosci* **25**, 7847–7857 (2005).

45. C. P. Bailey, F. L. Smith, E. Kelly, W. L. Dewey, G. Henderson, How important is protein kinase C in μ-opioid receptor desensitization and morphine tolerance? *Trends Pharmacol Sci* **27**, 558–565 (2006).

46. E. A. Johnson, S. Oldfield, E. Braksator, A. Gonzalez-Cuello, D. Couch, K. J. Hall, S. J. Mundell, C. P.

Bailey, E. Kelly, G. Henderson, Agonist-selective mechanisms of μ-opioid receptor desensitization in human embryonic kidney 293 cells, *Mol Pharmacol* **70**, 676–685 (2006).

47. X.-Y. Hua, A. Moore, S. Malkmus, S. F. Murray, N. Dean, T. L. Yaksh, M. Butler, Inhibition of spinal protein kinase Cα expression by an antisense oligonucleotide attenuates morphine infusion-induced tolerance, *Neuroscience* **113**, 99–107 (2002).

48. F. L. Smith, A. B. Lohmann, W. L. Dewey, Involvement of phospholipid signal transduction pathways in morphine tolerance in mice, *Br J Pharmacol* **128**, 220–226 (1999).

49. Y. Qiu, W. Zhao, Y. Wang, J.-R. Xu, E. Huie, S. Jiang, Y.-H. Yan, H. H. Loh, H.-Z. Chen, P.-Y. Law, FK506-binding protein 12 modulates μ-opioid receptor phosphorylation and protein kinase Cε-dependent signaling by its direct interaction with the receptor, *Mol Pharmacol* **85**, 37–49 (2014).

50. B. Feng, Z. Li, J. B. Wang, Protein kinase C-mediated phosphorylation of the μ-opioid receptor and its effects on receptor signaling, *Mol Pharmacol* **79**, 768–775 (2011).

51. J. Chu, H. Zheng, Y. Zhang, H. H. Loh, P.-Y. Law, Agonist-dependent μ-opioid receptor signaling can lead to heterologous desensitization, *Cell Signal* **22**, 684–696 (2010).

52. R. Winstel, S. Freund, C. Krasel, E. Hoppe, M. J. Lohse, Protein kinase cross-talk: membrane targeting of the β-adrenergic receptor kinase by protein kinase C, *Proc Natl Acad Sci U S A* **93**, 2105–2109 (1996).

53. P. Huang, W. Xu, S.-I. Yoon, C. Chen, P. L.-G. Chong, E. M. Unterwald, L.-Y. Liu-Chen, Agonist treatment did not affect association of μ opioid receptors with lipid rafts and cholesterol reduction had opposite effects on the receptor-mediated signaling in rat brain and CHO cells, *Brain Res*. **1184**, 46–56 (2007).

54. G. Gaibelet, C. Millot, C. Lebrun, S. Ravault, A. Saulière, A. André, B. Lagane, A. Lopez, Cholesterol content drives distinct pharmacological behaviours of μ-opioid receptor in different microdomains of the CHO plasma membrane, *Mol Membr Biol* **25**, 423–435 (2008).

55. L. Moulédous, S. Merker, J. Neasta, B. Roux, J.-M. Zajac, C. Mollereau, Neuropeptide FF-sensitive confinement of μ-opioid receptor does not involve lipid rafts in SH-SY5Y cells, *Biochem Biophys Res Comm* **373**, 80–84 (2008).

56. K. Suzuki, K. Ritchie, E. Kajikawa, T. Fujiwara, A. Kusumi, Rapid hop diffusion of a G protein-coupled receptor in the plasma membrane as revealed by single-molecule techniques, *Biophys J* **88**, 3659–3680 (2005).

57. F. Daumas, N. Destainville, C. Millot, A. Lopez, D. Dean, L. Salomé, Confined diffusion without fences of a G protein-coupled receptor as revealed by single particle tracking, *Biophys J* **84**, 356–366 (2003).

58. F. Daumas, N. Destainville, C. Millot, A. Lopez, D. Dean, L. Salome, Interprotein interactions are responsible for the confined diffusion of a G-protein-coupled receptor at the cell surface, *Biochem Soc T* **31**, 1001–1005 (2003).

59. A. Saulière, G. Gaibelet, C. Millot, S. Mazères, A. Lopez, L. Salomé, Diffusion of the μ-opioid receptor at the surface of human neuroblastoma SH-SY5Y cells is restricted to permeable domains, *FEBS Letters* **580**, 5227–5231 (2006).

60. A. Lopez, L. Salomé, Membrane functional organisation and dynamic of μ-opioid receptors, *Cell Mol Life Sci* **66**, 2093–2108 (2009).

61. D. D. Jensen, M. L. Halls, J. E. Murphy, M. Canals, F. Cattaruzza, D. P. Poole, T. Lieu, H.-W. Koon, C.

Pothoulakis, N. W. Bunnett, Endothelin-converting enzyme 1 and β-arrestins exert spatiotemporal control of substance P-induced inflammatory signals, *J Biol Chem* **289**, 20283–20294 (2014).

62. M. L. Halls, D. P. Poole, A. M. Ellisdon, C. J. Nowell, M. Canals, in *Methods in Molecular Biology*, (Springer New York, New York, NY), vol. 1335, pp. 131–161 (2015).

63. U. Klein, G. Gimpl, F. Fahrenholz, Alteration of the myometrial plasma membrane cholesterol content with β-cyclodextrin modulates the binding affinity of the oxytocin receptor, *Biochemistry* **34**, 13784–13793 (1995).

64. J. Schindelin, I. Arganda-Carreras, E. Frise, V. Kaynig, M. Longair, T. Pietzsch, S. Preibisch, C. Rueden, S. Saalfeld, B. Schmid, J.-Y. Tinevez, D. J. White, V. Hartenstein, K. Eliceiri, P. Tomancak, A. Cardona, Fiji: an open-source platform for biological-image analysis, *Nat Meth* **9**, 676–682 (2012).

65. E. Kardash, J. Bandemer, E. Raz, Imaging protein activity in live embryos using fluorescence resonance energy transfer biosensors, *Nat Prot* **6**, 1835–1846 (2011).

Acknowledgements

We thank D.D. Jensen for technical assistance, M.J. Christie for critical discussion and R.J. Summers, J.R. Lane and A.M. Ellisdon for careful review of this manuscript.

Designed the study: MLH, MC. Performed experiments: MLH, HRY, CJN, GLT, ABG, SC, DPP, MC. Analyzed and interpreted data: MLH, MC. Drafted and wrote manuscript: MLH, MC. Reviewed manuscript: all authors. Provided reagents: NWB, NAL.

This work was supported by a Monash Fellowship to MC, NHMRC RD Wright Fellowship to MLH (1061687), NHMRC Australia Fellowship to NWB (63303), NHMRC Project Grants (1011796, 1047633, 1049682, 1031886) to MC, MLH and NWB, ARC Centre of Excellence in Convergent Bio-Nano Science and Technology, Monash Institute of Pharmaceutical Sciences Large Grant Support Scheme grants to MC and MLH, and Monash University support to NWB; GLT is funded by DSTO Australia.

Figure Legends.

Figure 1. Ligand-dependent spatiotemporal signaling of MOPr. A-D, Spatiotemporal activation of ERK following vehicle, DAMGO or morphine stimulation. **(A)** Cytosolic ERK (416-606 cells). **(B)** Representative pseudocolor ratiometric images of cytoEKAR. **(C)** Nuclear ERK (561-810 cells). **(D)** Representative pseudocolor ratiometric images of nucEKAR. Pseudocolor scale as in B. **E-F** Spatiotemporal activation of PKC following vehicle, DAMGO or morphine stimulation. **(E)** Plasma membrane-localized PKC (155-220 cells). **(F)** Cytosolic PKC (45-115 cells). Symbols represent means, error bars SEM.

Figure 2. Effect of $G\alpha_{i/o}$ protein inhibition, β-arrestin knockdown or inhibition of endocytosis on cytosolic and nuclear ERK activation by MOPr. A-B, MOPr trafficking to early endosomes (n≥3) in response to 30 min vehicle, DAMGO or morphine in the presence of **(A)** the clathrin-mediated endocytosis inhibitor PitStop2 (PS2) or inactive control, or upon expression of wild-type (WT) dynamin or dominant negative dynamin K44E or **(B)** with and without knockdown of β-arrestins or pre-incubation with $G\alpha_{i/o}$ protein inhibitors. **C-F,** Spatial activation of ERK following vehicle, DAMGO or morphine stimulation, with and without knockdown of β-arrestins, $G\alpha_{i/o}$ protein inhibition, in the presence of PS2 or inactive control, or upon expression of WT or K44E dynamin. **(C)** Cytosolic ERK (19-168 cells) with $G\alpha_{i/o}$ protein inhibition or knockdown of β-arrestins. **(D)** Cytosolic ERK (35-245 cells) following inhibition of endocytosis. **(E)** Nuclear ERK (52-258 cells) with $G\alpha_{i/o}$ protein inhibition or knockdown of β-arrestins. **(F)** Nuclear ERK (51-306 cells) following inhibition of endocytosis. Bars/symbols represent means, error bars SEM. * $p<0.05$, ** $p<0.01$, *** $p<0.001$ versus vehicle control, two-way ANOVA with Tukey's multiple comparison test. AUC, area under the curve; scram., scrambled; β-arr., β-arrestin; PTx, pertussis toxin.

Figure 3. Role of PKC activation by morphine in the spatiotemporal control of ERK activity. **(A)** The effect of G protein inhibitors or inactive controls on plasma membrane PKC activity following vehicle, DAMGO or morphine stimulation (39-229 cells). **B-D,** MOPr spatiotemporal activation of ERK following vehicle,

DAMGO or morphine stimulation with or without inhibition of Gβγ or PKC. **(B)** Cytosolic ERK (31-101 cells). **(C)** Nuclear ERK (74-126 cells). **(D)** Nuclear ERK analyzed as area under the curve (AUC; 22-360 cells). **E-F,** MOPr trafficking (n≥3) following vehicle, DAMGO or morphine stimulation with or without inhibition of Gβγ or PKC. **(E)** MOPr-RLuc and Rab5a-Venus BRET. **(F)** MOPr-RLuc and KRas-Venus BRET. **G-I**, Effect of phosphorylation site mutations on MOPr regulation, trafficking and nuclear ERK. **(G)** MOPr-RLuc8 and β-arrestin-2-YFP BRET (n=3-7). **(H)** MOPr-RLuc8 and Rab5a-Venus BRET (n=3-4). **(I)** Nuclear ERK (87-359 cells). Bars/symbols represent means, error bars SEM. * $p<0.05$, ** $p<0.01$ and *** $p<0.001$ versus vehicle control, two-way ANOVA with Tukey's (A,D) or Dunnett's (E-I) multiple comparison tests. PTx, pertussis toxin; GFx, GF109203X; WT, wild-type.

Figure 4. DAMGO induces a unique MOPr distribution at the plasma membrane. Plasma membrane distribution of FLAG-MOPr in response to 10 min vehicle, DAMGO or morphine using GSD/TIRF (n=3-9). **(A)** Representative GSD/TIRF images and Euclidean distance maps (EDM) under control conditions. Scale bar 1 μm. **(B)** Average distance to nearest neighbor under control conditions. **(C)** Average distance to nearest neighbor following Gβγ inhibition. **(D)** Representative GSD/TIRF images and EDM following Gβγ inhibition. Scale bar 1 μm, pseudocolor scale as in A. **(E)** Representative GSD/TIRF images and EDM of wild-type MOPr (WT) or MOPr S375A under basal conditions. Scale bar 1 μm, pseudocolor scale as in A. **(F)** Average distance to nearest neighbor. Bars represent means, error bars SEM. *** $p<0.001$ versus vehicle control, one-way ANOVA with Dunnett's multiple comparison test (B,C) or unpaired t-test (E).

Figure 5. Disruption of membrane architecture alters MOPr signaling profiles. Spatiotemporal activation of PKC and ERK following vehicle, DAMGO or morphine stimulation, with and without pre-treatment with MβCD or MβCD/cholesterol complexes (MβCD/choles.). **(A)** Plasma membrane-localized PKC in response to DAMGO (40-174 cells). **(B)** Cytosolic ERK in response to DAMGO (30-167 cells). **(C)** Nuclear ERK in response to DAMGO (68-230 cells). **(D)** Plasma membrane-localized PKC in response to morphine (41-195

cells). **(E)** Cytosolic ERK in response to morphine (32-194 cells). **(F)** Nuclear ERK in response to morphine (80-217 cells). Symbols represent means, error bars SEM.

Figure 6. Spatiotemporal signaling of endogenous MOPr in DRG neurons. A-F, Spatiotemporal activation of ERK or PKC following vehicle, DAMGO or morphine stimulation. **(A)** Cytosolic ERK (56-120 neurons). **(B)** Nuclear ERK (45-64 neurons). **(C)** Plasma membrane-localized PKC (40-55 neurons). **(D)** Effect of PKC inhibition on cytosolic ERK (86-99 neurons). **(E)** Population analysis of the temporal profile of cytosolic ERK, with the number of neurons in each group indicated. **(F)** Effect of PKC inhibition on nuclear ERK (25-73 neurons). **G-I,** Plasma membrane distribution of endogenous MOPr in response to 10 min vehicle, DAMGO or morphine using GSD/TIRF (n=9-15). **(G)** Isolated DRG neuron immunostained for MOPr (green) and tubulin βIII (magenta). Scale bar 10 μm. **(H)** Representative GSD/TIRF images and Euclidean distance maps (EDM). Scale bar 1 μm. **(I)** Average distance to nearest neighbor. Bars/symbols represent means, error bars SEM. * $p<0.05$; ** $p<0.01$ and *** $p<0.001$ versus vehicle control, two-way ANOVA with Tukey's multiple comparison test (F) or one-way ANOVA with Dunnett's multiple comparison test (I). AUC, area under the curve.

Figure 7. Plasma membrane localization controls MOPr spatiotemporal signaling. (A) DAMGO causes recruitment of GRK2 and β-arrestin-2 (1), facilitating MOPr redistribution across the plasma membrane and transient activation of $G\alpha_{i/o}$-mediated cytosolic ERK and $G\alpha_{i/o}$-independent nuclear ERK (2). Upon prolonged stimulation of MOPr, DAMGO triggers MOPr clustering and receptor internalization via clathrin-coated pits (3) to early endosomes (4). **(B)** Morphine stimulates plasma membrane-localized Gβγ-PKCα that prevents receptor translocation within the plasma membrane. This causes a sustained activation of $G\alpha_{i/o}$-mediated cytosolic ERK (1). Inhibition of the Gβγ-PKCα-pathway, or alteration of plasma membrane organization facilitates MOPr translocation and activation of nuclear ERK by morphine (2) without receptor internalization.

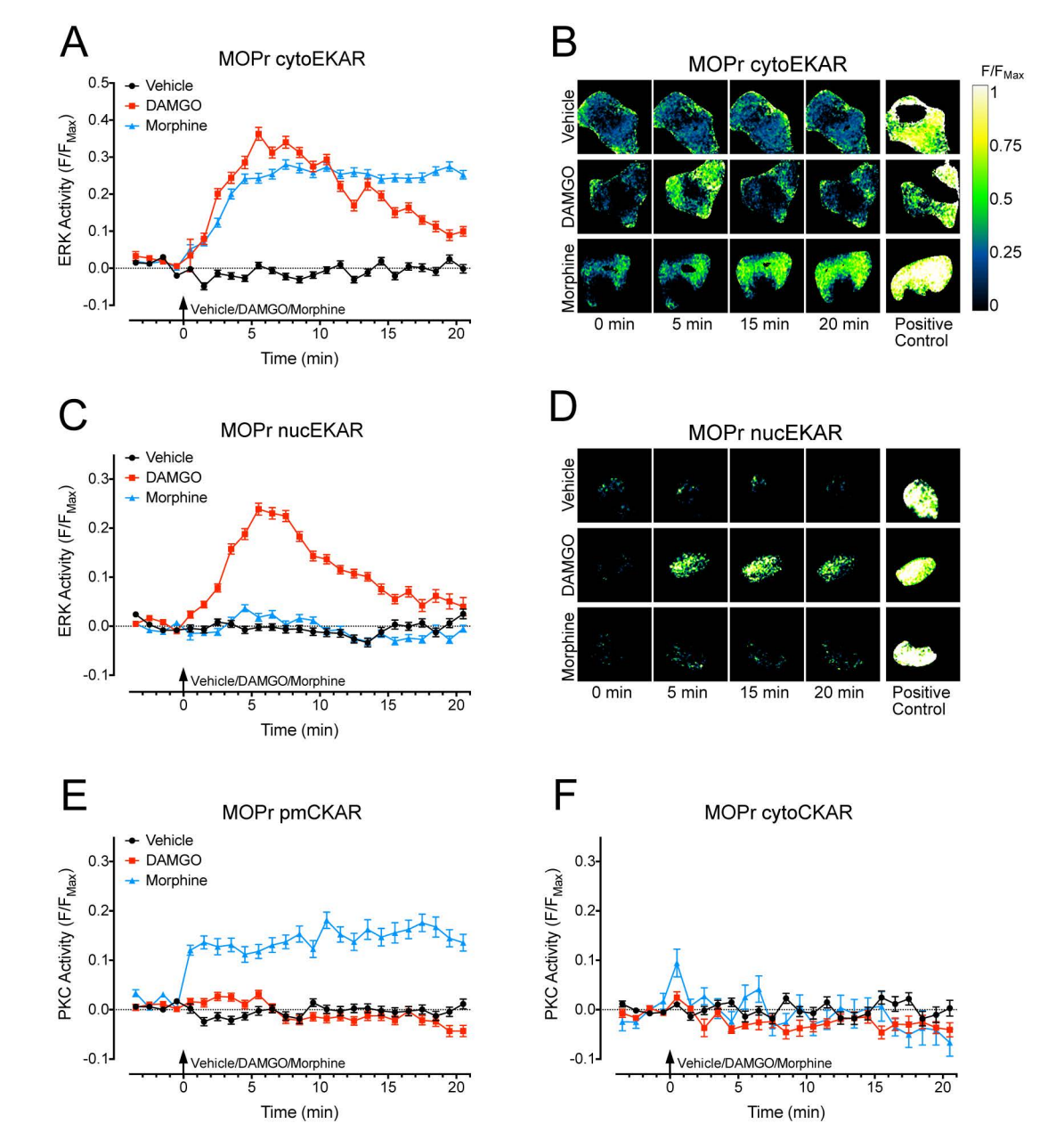
A
MOPr cytoEKAR
Vehicle
DAMGO
Morphine
ERK Activity (F/F$_{Max}$)
Vehicle/DAMGO/Morphine
Time (min)
B
MOPr cytoEKAR
F/F$_{Max}$
Vehicle
DAMGO
Morphine
0 min
5 min
15 min
20 min
Positive Control
C
MOPr nucEKAR
Vehicle
DAMGO
Morphine
ERK Activity (F/F$_{Max}$)
Vehicle/DAMGO/Morphine
Time (min)
D
MOPr nucEKAR
Vehicle
DAMGO
Morphine
0 min
5 min
15 min
20 min
Positive Control
E
MOPr pmCKAR
Vehicle
DAMGO
Morphine
PKC Activity (F/F$_{Max}$)
Vehicle/DAMGO/Morphine
Time (min)
F
MOPr cytoCKAR
PKC Activity (F/F$_{Max}$)
Vehicle/DAMGO/Morphine
Time (min)

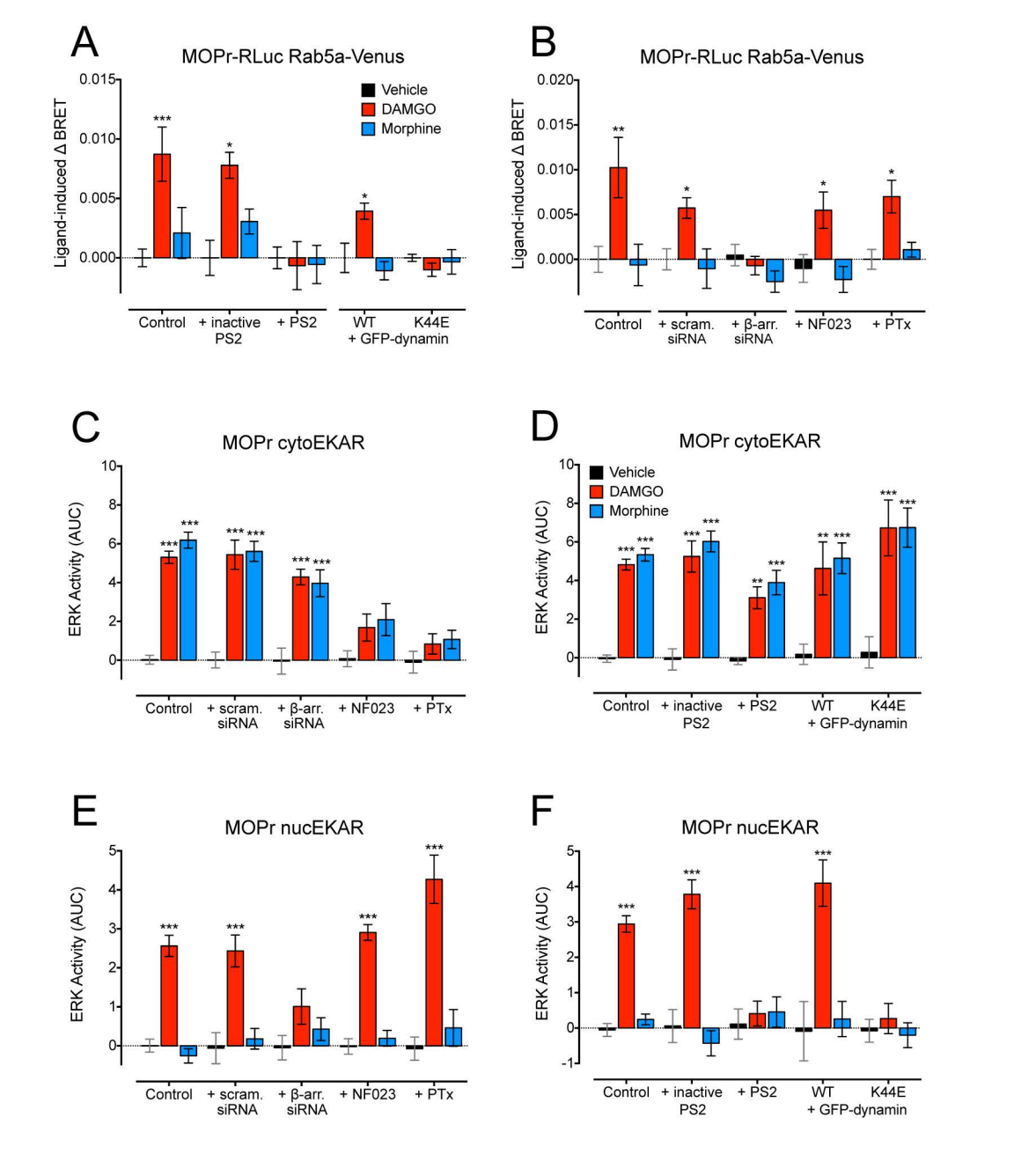
A
MOPr-RLuc Rab5a-Venus
Ligand-induced Δ BRET
Vehicle
DAMGO
Morphine
Control
+ inactive PS2
+ PS2
WT + GFP-dynamin
K44E
B
MOPr-RLuc Rab5a-Venus
Ligand-induced Δ BRET
Control
+ scram. siRNA
+ β-arr. siRNA
+ NF023
+ PTx
C
MOPr cytoEKAR
ERK Activity (AUC)
Control
+ scram. siRNA
+ β-arr. siRNA
+ NF023
+ PTx
D
MOPr cytoEKAR
ERK Activity (AUC)
Vehicle
DAMGO
Morphine
Control
+ inactive PS2
+ PS2
WT + GFP-dynamin
K44E
E
MOPr nucEKAR
ERK Activity (AUC)
Control
+ scram. siRNA
+ β-arr. siRNA
+ NF023
+ PTx
F
MOPr nucEKAR
ERK Activity (AUC)
Control
+ inactive PS2
+ PS2
WT + GFP-dynamin
K44E

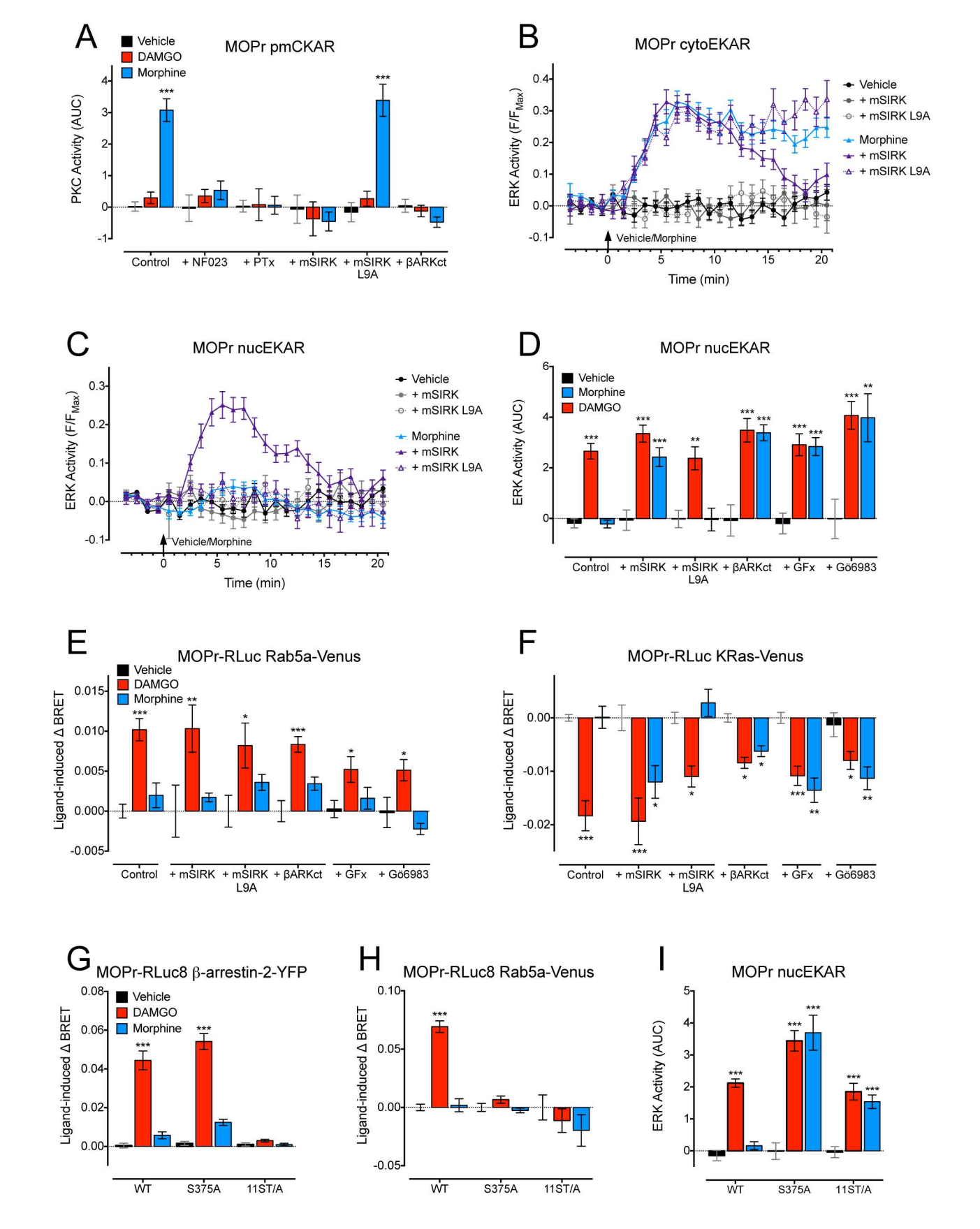
A
MOPr pmCKAR
Vehicle
DAMGO
Morphine
PKC Activity (AUC)
Control
+ NF023
+ PTx
+ mSIRK
+ mSIRK L9A
+ βARKct
B
MOPr cytoEKAR
ERK Activity (F/F_Max)
Vehicle
+ mSIRK
+ mSIRK L9A
Morphine
+ mSIRK
+ mSIRK L9A
Vehicle/Morphine
Time (min)
C
MOPr nucEKAR
ERK Activity (F/F_Max)
Vehicle
+ mSIRK
+ mSIRK L9A
Morphine
+ mSIRK
+ mSIRK L9A
Vehicle/Morphine
Time (min)
D
MOPr nucEKAR
Vehicle
Morphine
DAMGO
ERK Activity (AUC)
Control
+ mSIRK
+ mSIRK L9A
+ βARKct
+ GFx
+ Gö6983
E
MOPr-RLuc Rab5a-Venus
Vehicle
DAMGO
Morphine
Ligand-induced Δ BRET
Control
+ mSIRK
+ mSIRK L9A
+ βARKct
+ GFx
+ Gö6983
F
MOPr-RLuc KRas-Venus
Ligand-induced Δ BRET
Control
+ mSIRK
+ mSIRK L9A
+ βARKct
+ GFx
+ Gö6983
G
MOPr-RLuc8 β-arrestin-2-YFP
Vehicle
DAMGO
Morphine
Ligand-induced Δ BRET
WT
S375A
11ST/A
H
MOPr-RLuc8 Rab5a-Venus
Ligand-induced Δ BRET
WT
S375A
11ST/A
I
MOPr nucEKAR
ERK Activity (AUC)
WT
S375A
11ST/A

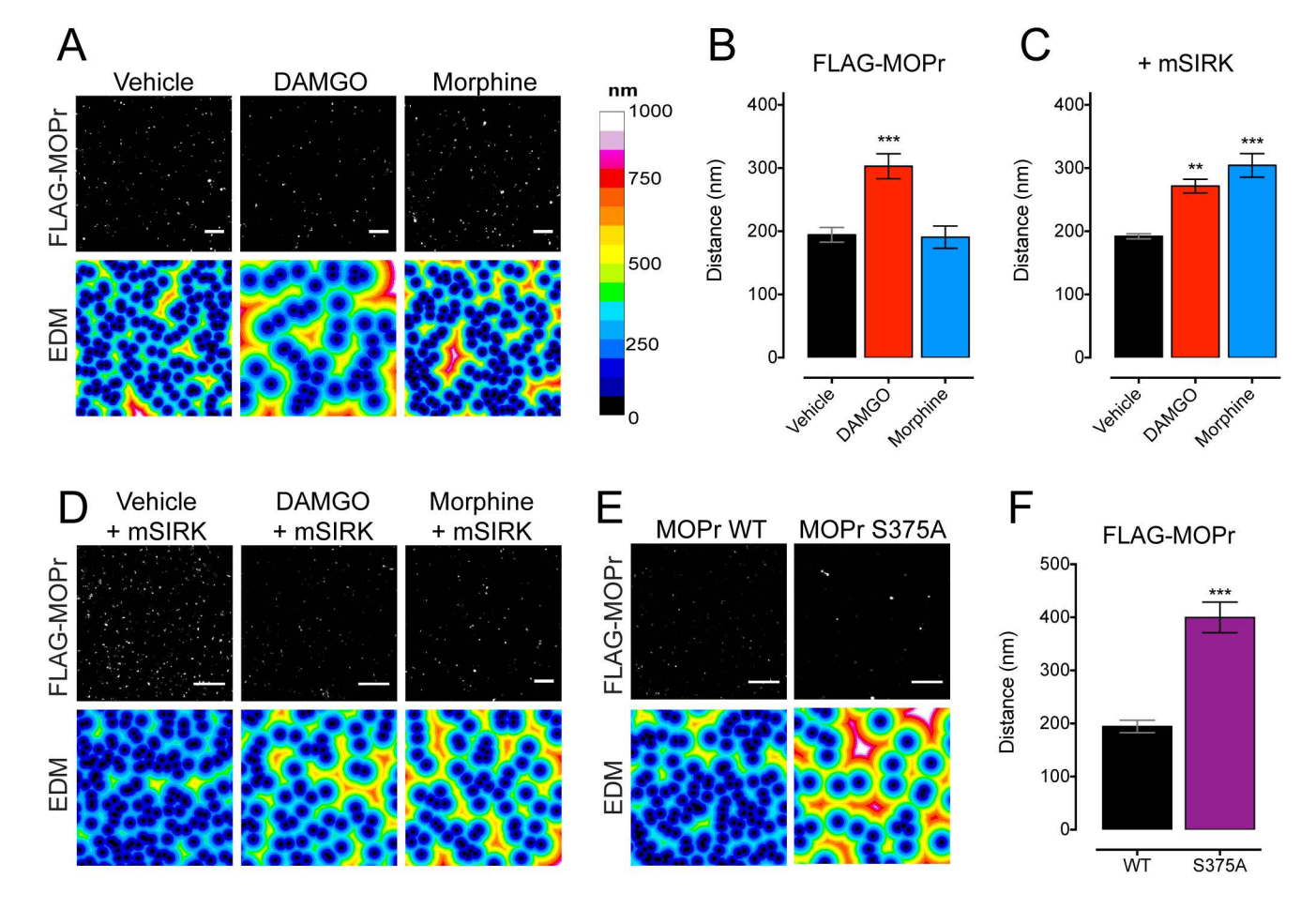
A
Vehicle
DAMGO
Morphine
FLAG-MOPr
EDM
nm
1000
750
500
250
0
B
FLAG-MOPr
Distance (nm)
400
300
200
100
0
***
Vehicle
DAMGO
Morphine
C
+ mSIRK
Distance (nm)
400
300
200
100
0
**
***
Vehicle
DAMGO
Morphine
D
Vehicle + mSIRK
DAMGO + mSIRK
Morphine + mSIRK
FLAG-MOPr
EDM
E
MOPr WT
MOPr S375A
FLAG-MOPr
EDM
F
FLAG-MOPr
Distance (nm)
500
400
300
200
100
0
***
WT
S375A

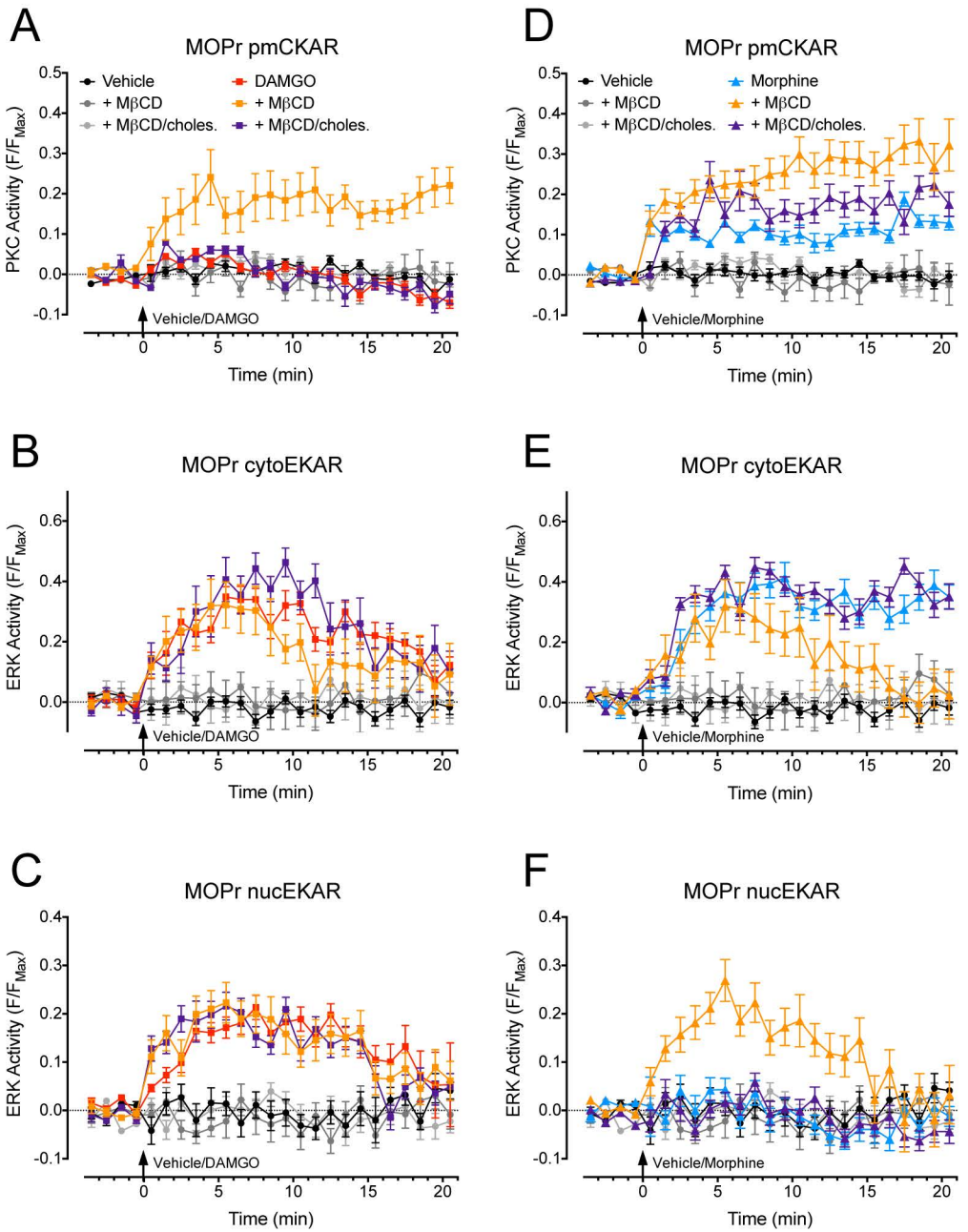
A
MOPr pmCKAR
Vehicle
+ MβCD
+ MβCD/choles.
DAMGO
+ MβCD
+ MβCD/choles.
PKC Activity (F/F$_{Max}$)
Vehicle/DAMGO
Time (min)
D
MOPr pmCKAR
Vehicle
+ MβCD
+ MβCD/choles.
Morphine
+ MβCD
+ MβCD/choles.
PKC Activity (F/F$_{Max}$)
Vehicle/Morphine
Time (min)
B
MOPr cytoEKAR
ERK Activity (F/F$_{Max}$)
Vehicle/DAMGO
Time (min)
E
MOPr cytoEKAR
ERK Activity (F/F$_{Max}$)
Vehicle/Morphine
Time (min)
C
MOPr nucEKAR
ERK Activity (F/F$_{Max}$)
Vehicle/DAMGO
Time (min)
F
MOPr nucEKAR
ERK Activity (F/F$_{Max}$)
Vehicle/Morphine
Time (min)

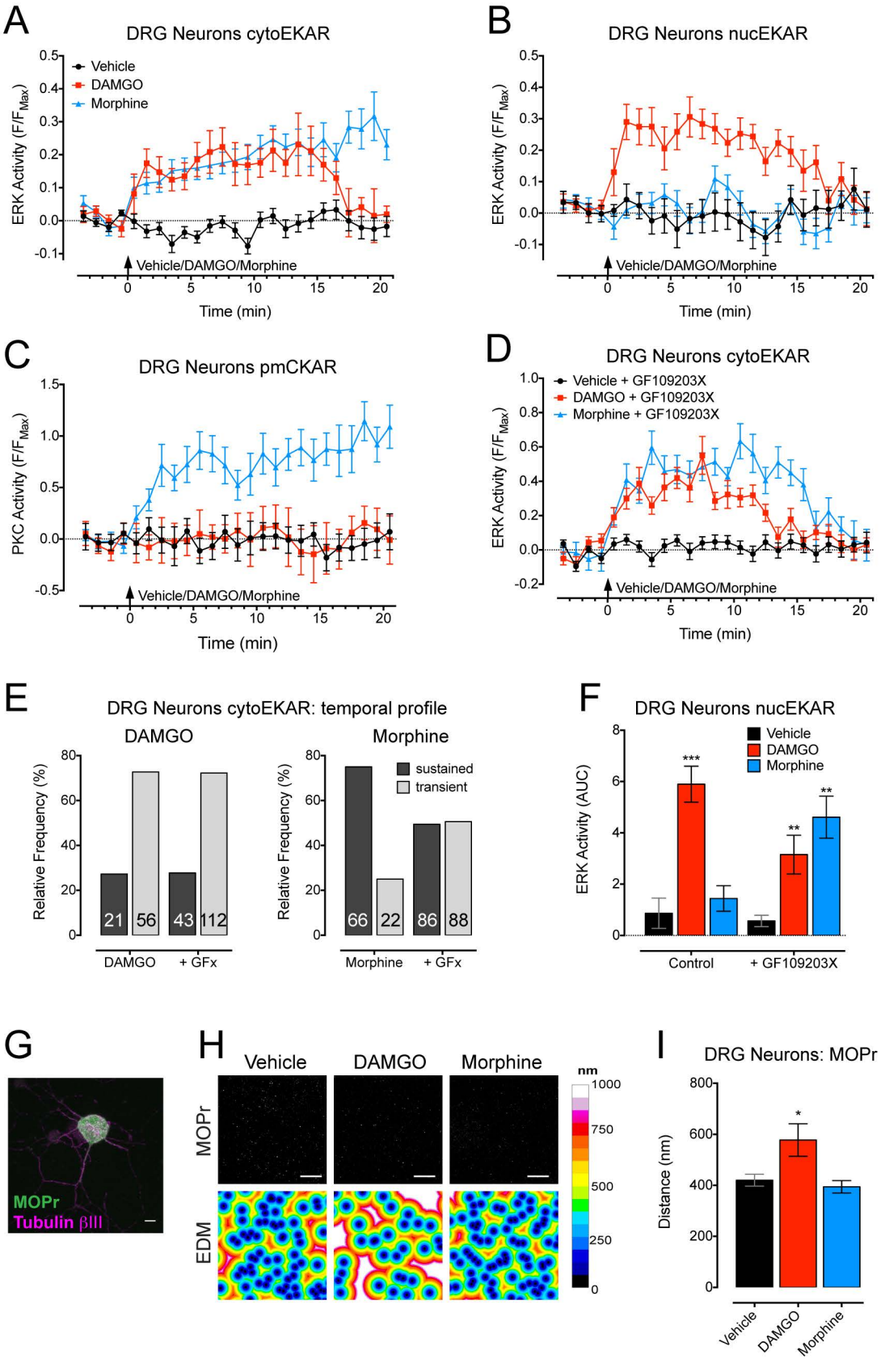
A
DRG Neurons cytoEKAR
Vehicle
DAMGO
Morphine
ERK Activity (F/F_Max)
Vehicle/DAMGO/Morphine
Time (min)
B
DRG Neurons nucEKAR
ERK Activity (F/F_Max)
Vehicle/DAMGO/Morphine
Time (min)
C
DRG Neurons pmCKAR
PKC Activity (F/F_Max)
Vehicle/DAMGO/Morphine
Time (min)
D
DRG Neurons cytoEKAR
Vehicle + GF109203X
DAMGO + GF109203X
Morphine + GF109203X
ERK Activity (F/F_Max)
Vehicle/DAMGO/Morphine
Time (min)
E
DRG Neurons cytoEKAR: temporal profile
DAMGO
Morphine
sustained
transient
Relative Frequency (%)
21
56
43
112
66
22
86
88
DAMGO
+ GFx
Morphine
+ GFx
F
DRG Neurons nucEKAR
Vehicle
DAMGO
Morphine
ERK Activity (AUC)
***
**
**
Control
+ GF109203X
G
MOPr
Tubulin βIII
H
Vehicle
DAMGO
Morphine
MOPr
EDM
nm
1000
750
500
250
0
I
DRG Neurons: MOPr
Distance (nm)
*
Vehicle
DAMGO
Morphine

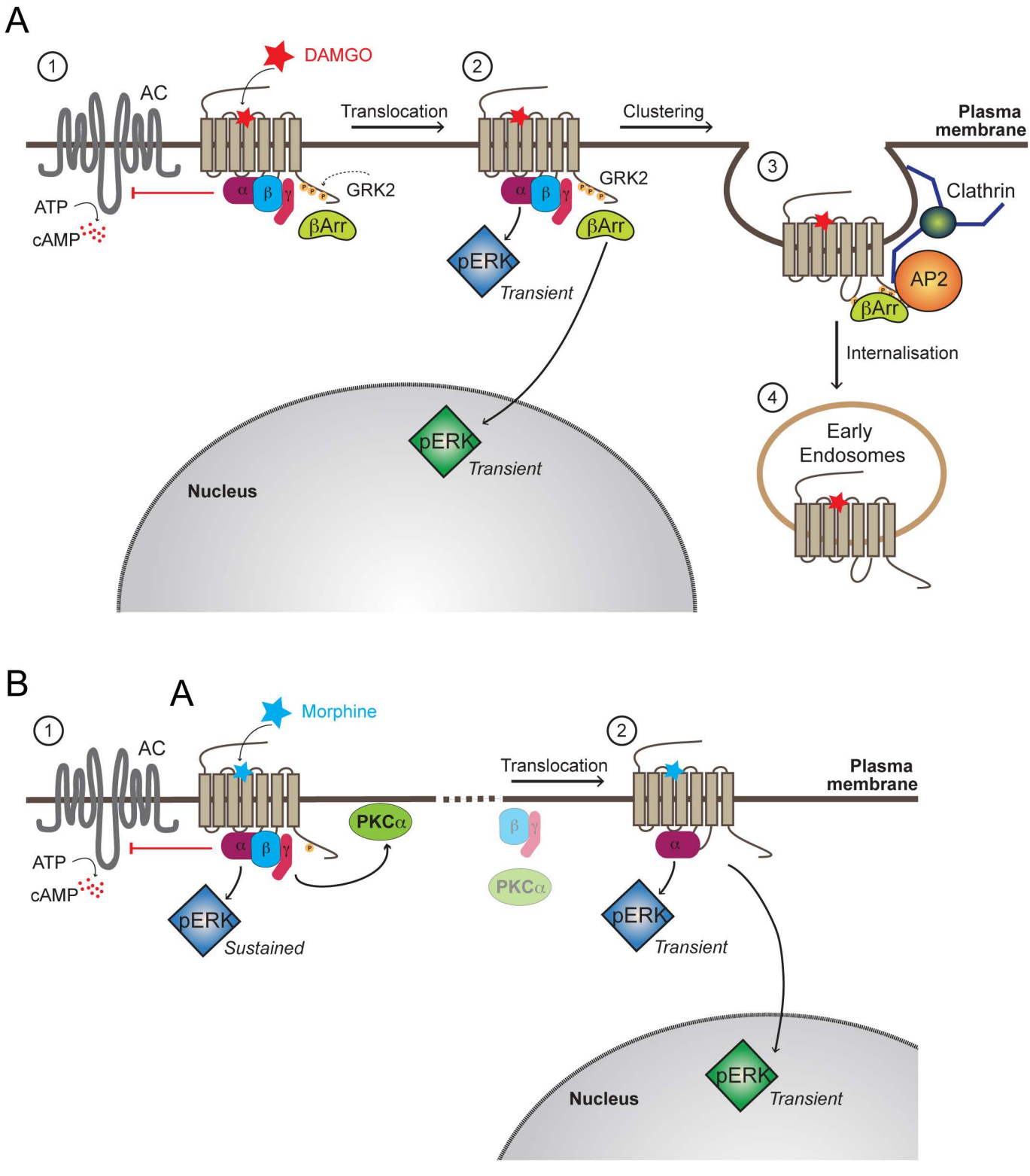
A
1
AC
DAMGO
ATP
cAMP
α
β
γ
GRK2
βArr
Translocation
2
GRK2
pERK
Transient
Clustering
Plasma membrane
3
Clathrin
AP2
βArr
Internalisation
4
Early Endosomes
pERK
Transient
Nucleus
B
A
1
AC
Morphine
ATP
cAMP
α
β
γ
PKCα
pERK
Sustained
Translocation
2
Plasma membrane
β
γ
PKCα
α
pERK
Transient
Nucleus
pERK
Transient